JOURNAL OF CATALYSIS **178,** 14–25 (1998)
ARTICLE NO. CA982114

Oxygen Storage Dynamics in $Pt/CeO_2/Al_2O_3$ Catalysts

Anna Holmgren and Bengt Andersson[1]

Department of Chemical Reaction Engineering, Chalmers University of Technology, S-412 96 Göteborg, Sweden

Received March 10, 1997; revised March 4, 1998; accepted April 21, 1998

The oxidation; the $^{16}O_2$, $^{18}O_2$, $^{16}O^{18}O$ isotopic equilibration; the isotope oxygen exchange; and the reduction by CO were studied on Pt/CeO_2, $Pt/CeO_2/Al_2O_3$, Pt/Al_2O_3, and CeO_2 catalysts at 200–600°C. On a 0.1-s residence time scale, the oxidation occurred instantly on all samples. The rates of oxygen exchange and equilibration were closely related, which shows that the rate-determining step in the oxygen storage is the adsorption and desorption of oxygen. The oxygen exchange was faster on the alumina-supported catalysts than on the ceria-supported catalysts; however; the amount of oxygen that could be exchanged was higher on Pt/CeO_2 and CeO_2. On Pt/Al_2O_3, the amount of exchange corresponds to the expected number of OH groups. The exchange rate was found to be strongly dependent on the Pt content on the alumina-supported catalysts, but almost independent of the Pt content on the ceria-supported catalysts. This indicates that the oxygen exchange does not proceed via Pt, but occurs directly on ceria. The reduction of ceria by CO at 300–650°C was increased by Pt. A model for the reduction of Pt/ceria with CO is presented. The model contains three types of CO consuming reactions, two on ceria and one which also involves Pt. CO chemisorption on Pt/CeO_2 at 25°C resulted in large CO uptakes, a part of which is probably due to CO uptake on ceria. For metal dispersion measurements, a method for subtracting the ceria contribution is suggested.

INTRODUCTION

The capacity to store and release oxygen is a crucial property of the car-exhaust purification catalyst. Thanks to this capacity, the catalyst can maintain a high conversion for both reduction and oxidation reactions during deviations from the desired stoichiometric exhaust gas mixture. The variations around stoichiometry in the exhaust occur on two time scales. One is shorter than 1 s long and corresponds to the time lag of the lambda sensor control system. The other is about 0.01–0.06 s long and corresponds to varying composition in the exhaust from the different cylinders. This high-frequency oscillation has a lower amplitude than the time-lag oscillation.

Oxygen-storing components, such as ceria, have been used in car-exhaust catalysts since the early 1980s. Since then, their functions have been studied extensively. In an early study, Yao and Yu Yao (1) defined the fast oxygen storage capacity (OSC) as the oxygen uptake during an O_2 pulse following a pulse of CO. They found no OSC on ceria at 300°C and very little at 400°C. This is consistent with the fact that surface oxygen in ceria cannot be reduced below 300–350°C (1, 2). However, when Pt, Pd, or Rh was added to a ceria/alumina catalyst, there was substantial OSC even at 300°C (1). Accordingly, it has been shown that the presence of Rh, Pt, or Pd lowers the temperature of the surface ceria reduction peak to about 200–300°C (1–3).

Yu Yao (4) found an increased activity for oxidation of CO on Pt or Pd samples that had been reduced in CO above 300°C. Furthermore, Yu Yao (4) noted that the presence of ceria changed the kinetics in the oxidation of CO and of some hydrocarbons at net oxidizing or stoichiometric conditions. An interesting phenomenon was that the self-inhibiting effect of CO decreased. Pt/CeO_2 has also been found to have improved light-off properties compared to Pt/Al_2O_3, but only after a high-temperature reduction (3, 5, 6). The importance of having a large contact area between Pt and CeO_2 was shown by Nunan *et al.* (7). These authors correlated both light-off activity of CO and HC, and the synergistic reduction of Pt and ceria, to the degree of Pt/ceria interaction. The interaction was varied by ceria loading and crystallite size.

The isotopic equilibration and exchange of oxygen, which we have used in this study, is useful for examining the activation of dioxygen (8). Abderrahim and Duprez (9) measured the oxygen diffusion rate on different supports by exchanging $^{18}O_2$ in the gas phase with ^{16}O in the support. They found that on Pt/Al_2O_3, the dissociative adsorption and desorption of oxygen are the rate-limiting steps in the oxygen exchange, which is also believed to be the case for CeO_2 (10). On Rh/Al_2O_3, the exchange rate was found to be about four times higher (9), and therefore, the oxygen surface diffusion became the rate-determining step in the exchange above 350°C. Martin *et al.* (11) measured the oxygen exchange and the OSC on $Pt–Rh/CeO_2–Al_2O_3$ catalysts and found a strong correlation between these two values.

Our aim was to study the capacities and rates for oxidation and reduction of Pt/ceria/alumina model catalysts. A key mechanism that we focused on was the transport of oxygen, both the adsorption/desorption step and the

[1] To whom correspondence should be addressed.

0021-9517/98 $25.00

surface and bulk diffusion. The investigation can be divided into three major parts:

(1) Measurements of oxygen consumption in oxidation and of CO consumption in reduction. These measurements were done to determine the total oxygen storage capacity and to find out whether it is the reduction or the oxidation that determines the capacity. The measurements were carried out as step changes, which give total consumption, and also, from the shapes of the step responses, reaction rates.

(2) Exchange of ^{18}O into the catalyst to try and determine the rate of oxygen diffusion into the material.

(3) $^{16}O_2$ and $^{18}O_2$ equilibration to $^{16}O^{18}O$ to measure the rate of oxygen dissociation.

In order to understand the basic mechanisms of oxygen storage, we used few-component gases that were dry and sulfur-free. In the real car exhaust, the high concentrations of, e.g., water, carbon dioxide, and sulfur may affect the oxygen storage. As an example, Padeste *et al.* (12) have shown that the reduction of bulk ceria by hydrogen is thermodynamically hindered at the typical H_2O partial pressures and temperatures of car exhaust.

During the standard CO chemisorption measurement for determining the Pt dispersion, we obtained very high values for the Pt/ceria catalysts, which indicate that the method is not suitable for determining metal dispersion on ceria-supported catalysts. Therefore, we also did further studies of the interaction of CO with Pt/ceria.

EXPERIMENTAL METHODS

Catalyst Samples

The catalyst samples consisted of Pt supported on Al_2O_3, CeO_2, or Al_2O_3/CeO_2. Two Pt loadings were used, one of 0.25–0.3% Pt, and one of 2–3% Pt. Unpromoted Al_2O_3 and CeO_2 were also used. Two types of CeO_2, with different surface area, were used. The higher surface area sample was from Rhône–Poulenc (Cerium oxide 99.5 H.S.A. 514). It was calcined at 600°C and is referred to as CeO_2 (HS). The lower surface area powder was calcined at 500°C and is referred to as CeO_2 (LS). The Pt/CeO_2 samples were prepared by impregnating the CeO_2 with a solution of H_2PtCl_6, and then freeze-drying the impregnated sample overnight before calcination at 500°C. A chlorine-free Pt/CeO_2 sample was also prepared from impregnating CeO_2 with a basic solution of $Pt(NH_3)_4(OH)_2$, and then freeze-drying and calcinating the sample. For the $Pt/CeO_2/Al_2O_3$ catalysts, the alumina was impregnated by an aqueous solution of $Ce(NO_3)_3$. Pt was then introduced through H_2PtCl_6 impregnation. The Pt/Al_2O_3 catalysts were prepared by H_2PtCl_6 impregnation of the alumina. The $Pt/CeO_2/Al_2O_3$ and Pt/Al_2O_3 samples were calcined at 500°C. Catalyst characteristics are shown in Table 1. In each experiment, 0.05–0.1 g of catalyst was used.

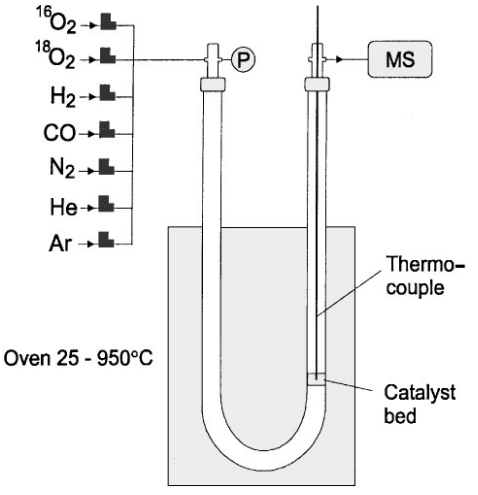

FIG. 1. Experimental setup.

Experimental Setup

The catalysts were investigated in a flow reactor system shown in Fig. 1. The gases were purified by water and oxygen traps; the latter was used only for the gases that did

TABLE 1

Catalyst Characteristics

Sample	Pt dispersion from the CO chemisorption (CO/Pt)	Pt dispersion from H_2 chemisorption (H/Pt)	Surface Pt according to the CO chemisorption (μmol/g catalyst)	BET surface area (m^2/g)
2.9% Pt/CeO_2 (HS)	0.7	0.41	100	158
2.9% Pt/CeO_2[a] (HS)	0.9	—	130	—
0.3% Pt/CeO_2 (HS)	1.4	0.72	20	—
2.0% Pt-19.6% CeO_2(LS)/Al_2O_3	0.1	—	10	126
0.25% Pt-1% CeO_2(LS)/Al_2O_3	0.24	—	3	—
0.25% Pt/Al_2O_3	1.0	—	13	—
2.5% Pt/Al_2O_3	0.2	0.16	28	151
CeO_2 (LS)	—	—	0	75
CeO_2 (HS)	—	—	0	200

[a] Prepared from a chlorine-free Pt precursor.

not contain oxygen or carbon monoxide. The gas flow rates were controlled by mass flow controllers. The powder catalyst was placed in a tubular quartz reactor in an oven. Thermocouples in the catalyst bed and in the gas were used to measure and control the temperature. The composition of the gas at the reactor outlet was measured by a mass spectrometer (Fisons Gaslab 300). A heated silica capillary was used to sample the gas. All experiments were carried out at atmospheric pressure.

Oxidation and Oxygen Exchange

In the step-response oxidation experiments, the sample was first oxidized in 25 nml/min (at 20°C, 1.01325 bar) of 10% $^{16}O_2$ in Ar at 400°C for 1 h, and then reduced in 25 nml/min of 5% H_2 in Ar for 1 h, at 400 or 650°C. In some experiments, the reducing gas was 4.37% CO in Ar. The sample was then cooled to reaction temperature in argon flow. During the cooling, a steady flow of 25 nml/min of an oxygen isotope mixture was established. The isotope mixture contained about 0.4% $^{16}O_2$, 0.4% $^{18}O_2$, and 0.5% $^{16}O^{18}O$ in Ar, and 1–5% of nitrogen to detect the gas hold-up time. The flow was then switched from Ar to the isotopic mixture. The contact time between the reactants and the catalyst was between 0.07 and 0.2 s, in response to the gas flow rate and the density of the powder catalyst. In some experiments, the sample was oxidized in $^{16}O_2$, before the isotopic mixture was introduced. By this procedure, the exchange between gas oxygen and bulk oxygen could be separated from the exchange between gas oxygen and surface oxygen.

CO Reduction

In the CO reduction step changes, the samples were reduced in 25 nml/min of 5% H_2 in Ar at 400°C for 1 h, and then oxidized in 25 nml/min of 10% O_2 in Ar for 30 min. After cooling in Ar, the flow was switched to 25 nml/min of either a mixture of 0.38% CO in Ar with He as an inert tracer, or a mixture of 4.37% CO in Ar. Two different CO concentrations were used to so that kinetic and mass transfer rates could be more easily studied. The CO step was terminated when there was no longer any substantial CO uptake, which gave a duration of each step of 20–60 min. The concentrations of CO, CO_2, O_2, Ar, and He were detected.

Oxygen Equilibration

In the oxygen equilibration experiments, the samples were reduced in 5% H_2 in Ar at 400°C for 1 h and then oxidized in 25 nml/min of a mixture of 0.5% $^{16}O_2$ and 0.5% $^{18}O_2$, or 1% $^{16}O_2$ and 1% $^{18}O_2$ at 500–600°C. The oxidation was continued until steady state in the rate of $^{16}O^{18}O$ formation was reached, i.e., until the exchange between the gas phase and the catalyst was completed. The steady-state rate was then recorded continuously during cooling until the $^{16}O^{18}O$ formation stopped.

CO Chemisorption

The amount of irreversible CO chemisorption was measured at 25°C. The catalyst was first reduced in 100 nml/min of H_2 at 300 or 650°C for 1 h and then cooled to room temperature in 100 nml/min of Ar and 5 nml/min of H_2, before the admission of 100 nml/min of 98 ppm CO in N_2. After the surface had been saturated with CO, the sample was swept with Ar for 7 min, before the CO adsorption procedure was repeated. The amount of irreversibly adsorbed CO was taken as the difference between the two runs. The concentration of CO in the outflow was detected by an IR analyzer for CO (ADC).

CO-TPD

Temperature-programmed desorption was conducted on 2.9% Pt/CeO_2 after CO chemisorption at 25°C, according to the procedure described above. Then 100 nml/min of Ar was flown through the sample, which was heated from 25 to 550°C with a temperature ramp of 20 K/min. The concentrations of CO and CO_2 were detected, by means of an IR analyzer and an MS, respectively.

H_2 Chemisorption

The amount of irreversible H_2 chemisorption was measured at 30°C. First, the sample was heated to 150°C in vacuum, then purged with He at 150°C for 30 min, and then heated in vacuum to 350°C. Next, the sample was reduced in H_2 at 350°C for 1 h, heated to 400°C in vacuum, and outgassed at 400°C for 1 h. The sample was then cooled to room temperature and exposed to H_2 flow until no H_2 uptake was observed. Finally, the sample was outgassed at 30°C for 1 h and again exposed to H_2 at 30°C. The amount of irreversible chemisorption was taken as the difference in adsorbed amount of H_2 between the two adsorption steps.

RESULTS

Oxidation

Figure 2 shows the concentrations in the outflow when 2.0% $Pt/CeO_2/Al_2O_3$, which has been reduced in H_2 at 400°C, is exposed to an isotope mixture of oxygens. Initially, all oxygen is consumed in adsorption and oxidation of the reduced catalyst. The oxygen uptake is the area between the normalized N_2-tracer concentration and the total oxygen concentration. As can be seen in Fig. 2, the oxidation is fast relative to the gas hold-up time. The total amount of oxygen consumed at 300 and 400°C, after a reduction in H_2 at 400°C, is shown in Fig. 3.

This amount shows how much oxygen can be stored on the reduced catalyst. Pt/CeO_2 is the most efficient storing

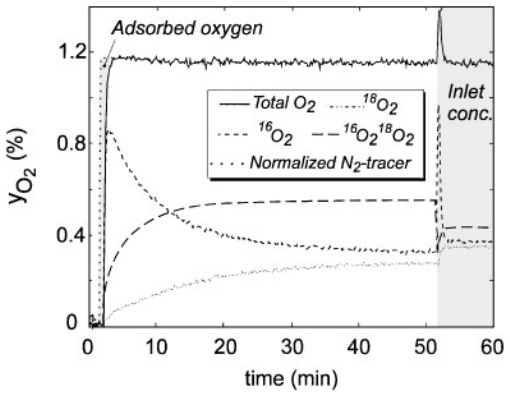

FIG. 2. Isotopic oxygen step on 2.0% $Pt/CeO_2/Al_2O_3$ at 400°C.

material. There is also a higher oxygen consumption on the higher Pt loading sample (2.9% Pt/CeO_2) compared to the lower Pt loading sample (0.3% Pt/CeO_2). This difference remains even if the contribution of oxygen storage on Pt is subtracted, which for these two catalysts is approximately 100 and 20 μmol/g respectively (see Table 1), assuming that one exposed (and reduced) Pt atom can adsorb one oxygen atom. Such an increase in oxygen consumption with increased Pt loading on Pt/CeO_2 was earlier observed by Yao and Yu Yao (1). In contrast, Schlatter and Mitchell (13) found an increased oxidation rate due to the addition of Pt to a 5% CeO_2/Al_2O_3 catalyst, but no additional total oxygen uptake. From Fig. 3 it is also seen that Pt/Al_2O_3, as expected, is a poor oxygen-storage catalyst. On this catalyst, the oxygen stored roughly corresponds to one oxygen atom per exposed Pt atom, the latter according to the CO chemisorption measurement; see Table 1. Thus, there is no additional storage in the alumina support. It is difficult to explain the larger uptake of 0.25% Pt/Al_2O_3 compared to 2.5% Pt/Al_2O_3. Therefore, we have to attribute it to experimental errors. $Pt/CeO_2/Al_2O_3$ is between Pt/Al_2O_3 and Pt/CeO_2 in terms of oxygen-storage capacity. At 300°C, the relation between the oxygen uptake and the ceria loading is 0.13 O atoms per cerium oxide molecule on 2.9% Pt/CeO_2, 0.08 on 0.25% Pt/CeO_2, 0.11 on $Pt/CeO_2/Al_2O_3$, and 0.03 on CeO_2. These figures indicate that Pt facilitates the reduction/oxidation of ceria in the $Pt/CeO_2/Al_2O_3$ sample, but somewhat less efficiently than in Pt/CeO_2, because a smaller fraction of the ceria is in direct contact with Pt when there is also alumina present.

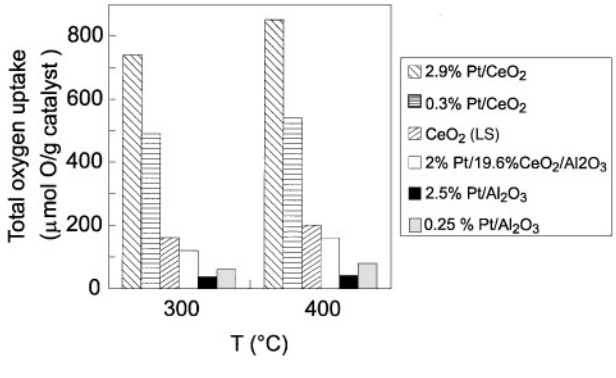

FIG. 3. Total oxygen uptake at 300 and 400°C after reduction in hydrogen at 400°C.

For all samples, the amount of oxygen uptake is higher at 400°C than at 300°C; see Fig. 3. The increase is between 10 and 33%. Since the reductive pretreatment is the same, this suggests that an oxidation temperature of 300°C is not sufficient to saturate a sample which has been reduced at 400°C. Accordingly, reducing the Pt/CeO_2 catalyst further, at 650°C, does not increase the oxygen uptake at 400°C. This is not due to sintering as one might suspect, because the oxygen uptake after reduction at 400°C was only slightly lowered when repeated after the reduction at 650°C. In a temperature-programmed oxidation of this high-temperature reduced sample, see below, a temperature of 500–600°C was required for complete reoxidation to occur.

Reduction

Table 2 shows the CO consumption during the reduction step. In some experiments, the CO_2 production during step (I) and the CO_2 production during a subsequent oxidation (II) at the same temperature as the CO step were also measured. From Table 2 it can be see that, on all catalysts, not all CO that is taken up by the catalyst results in immediate CO_2 production. The same observation was made by Taha *et al.* (14) on a commercial Pt/Rh catalyst containing 6.3% ceria at temperatures below 350°C. At 450°C and above, the amount of CO consumption and CO_2 production was the same. Due to this temperature dependency, these authors attributed the difference in CO consumption and CO_2 production to CO_2 adsorption on the ceria. This is supported by the observation that CO and CO_2 adsorption on ceria results in various carbonate and carboxylate species (15–17), some of which are strongly bound. In the present study, CO_2 adsorption on ceria and alumina does not seem to be the only explanation to the small CO_2 production, since there is no clear temperature trend. Moreover, most of the CO uptake that does not immediately become CO_2 will produce CO_2 during a subsequent oxidation; see Table 2. If CO_2 was adsorbed on the support, it is not likely to desorb only because the atmosphere is altered to oxidizing. Instead, our data are best explained by CO adsorption and carbon depositions from the CO disproportionation reaction.

Reduction of Pt/CeO_2. Reduction at 300 and 400°C occurs quite easily on the Pt-containing catalysts. Figure 4a shows the relatively fast reduction of 2.9% Pt/CeO_2. At first, there is a complete consumption of CO. Then follows a period of partial CO consumption, and finally saturation in the CO uptake is reached. The dependency of the CO uptake on the partial pressure of CO during the step is small, see Table 2, which indicates that saturation of the oxygen

TABLE 2

CO Uptake and CO_2 Production (μmol/g catalyst) in a Step Reduction at 300 and 400°C

Sample	Temp. (°C)	CO partial pressure	CO uptake	CO_2 production (I)	CO_2 production (II)
2.9% Pt/CeO_2	300	4.37%	870–1000	560–680	220
	300	0.38%	850	690	—
	400	4.37%	860	590–750	120
	400	0.38%	860–1010	770	—
	650	4.37%	1660	1260	530
2.0% $Pt/CeO_2/Al_2O_3$	300	4.37%	400	330	110
	300	0.38%	250	—	—
	400	4.37%	510–760	540	260
	400	0.38%	230	—	—
2.5% Pt/Al_2O_3	300	4.37%	190	120	80
	300	0.38%	120	60	—
	400	4.37%	370	320	120
	400	0.38%	250–280	240	40
CeO_2	300	4.37%	370	150	—
	300	0.38%	130	—	—
	400	4.37%	830–1020	450–470	310–340
	400	0.38%	480	—	—
	650	4.37%	830–1130	420–760	220

Note. All samples were preoxidized at 400°C.

removal is reached within the CO step time at both CO partial pressures.

It is interesting to compare the amount of CO consumption/CO_2 production to the amount of CeO_2, in order to find out how much of the ceria can be reduced at these temperatures. We assume that ceria is reduced from Ce(+4) to Ce(+3), a reduction which has been detected in XPS measurements on $Pt/CeO_2/Al_2O_3$ after similar reduction treatments (18). From the BET data in Table 1, and the assumption of spherical ceria crystals, the proportions of oxygen atoms in the ceria lattice that are in surface position can be calculated. For 2.9% Pt/CeO_2, 31% of the oxygen atoms are at the surface. The CO_2 production (I) of 2.9% Pt/CeO_2 at 300 and 400°C is equivalent to about 25% of the CeO_2 being reduced to $CeO_{1.5}$. Thus, it seems likely that only surface ceria is reduced at 300–400°C, especially when considering that part of the CO_2 production may come from the water–gas–shift reaction between CO and OH groups on ceria.

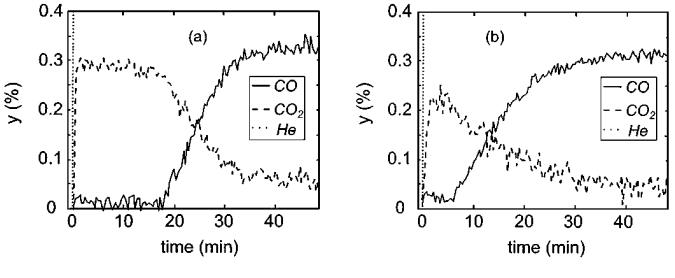

FIG. 4. CO step change at 400°C on (a) 2.9% Pt/CeO_2 and (b) CeO_2 (HS).

Between 300 and 400°C the total CO consumption is independent of temperature. However, the CO uptake at 650°C is almost doubled; see Table 2. At this temperature, a partial reduction of the bulk of ceria is possible (1, 19). The difference in CO uptake and CO_2 production is very large (1660 and 1260 μmol/g, respectively), indicating that carbon is stored on the catalyst, as C or as strongly adsorbed CO and CO_2. Due to the large CO/CO_2 discrepancy at 650°C, the nature of the reduction by CO at 650°C was investigated further in temperature-programmed oxidation (TPO) and temperature-programmed desorption (TPD) from 40 to 650°C, with a temperature ramp of 40 K/min. We found that during the temperature-programmed oxidation, some CO_2 was desorbed below 450°C, and about 300 μmol/g catalyst between 500 and 650°C. There was also some CO desorption. The oxygen uptake at these temperatures roughly matched the CO_2 formation, in that one oxygen molecule was consumed for each desorbed CO_2 molecule. Thus, very little of the oxygen in the desorbed CO_2 came from the catalyst. During the temperature-programmed desorption, very small amounts of CO_2 were desorbed. Our interpretation of these results is that CO is deposited on the catalyst mainly as carbon residues, which below 650°C can be removed only by oxidation. The measured high Pt dispersion after oxidation at 300°C, see below, indicates that this temperature is sufficient to clean the Pt surface by oxidation of CO and carbon. However, for carbon on ceria, higher temperatures are required for oxidation.

Reduction of CeO_2. On pure ceria, the reduction is slower and does not produce as much CO_2; see Fig. 4b. The slow reaction rate is also shown by the temperature influence: the CO consumption is considerably higher at 400°C than at 300°C; see Table 2. Furthermore, this catalyst has the largest difference in CO uptake between the two CO concentrations used (4.37 and 0.38%). This is an indication of the slower reduction rate in the absence of Pt. On ceria, unlike the other catalysts, there is also a trend of a larger CO uptake compared with the total CO_2 production (I + II). A possible explanation for this is that carbon depositions on ceria, caused by CO disproportionation, would be more difficult to oxidize in the absence of Pt.

Reduction of Pt/Al_2O_3 and $Pt/CeO_2/Al_2O_3$. Pt/Al_2O_3 also has some CO uptake capacity; see Table 2. The CO uptake is almost twice as high at 400°C than at 300°C. The strong temperature dependence indicates that part of the CO consumption is from the water–gas–shift reaction, which has been found to occur even on unpromoted alumina at and above 400°C (5). The highest CO_2 production on Pt/Al_2O_3 (320 μmol/g; see Table 2) would correspond to a surface concentration of 1.3 OH groups/nm^2 alumina, if all CO_2 were produced in the water–gas–shift reaction. This is a realistic concentration, of the same magnitude as the amount of OH groups determined by the oxygen exchange at 400°C on the same catalyst (3.1 OH groups/nm^2 alumina; see below). When repeating the CO step change on 2.5% Pt/Al_2O_3 with a subsequent oxidation, the CO uptake at 400°C decreased from 280 to 170 and then to 80 μmol/g catalyst. Thus, the CO uptake seemed to approach the amount of surface Pt (28 μmol/g catalyst; see Table 1). This is also an indication of that any additional CO consumption is due to reaction with OH groups on alumina, since the continuous lowering of the CO uptake points to a depletion of OH groups rather than some other explanation such as an oxygen leak in the reactor system.

The amount of CO uptake on $Pt/CeO_2/Al_2O_3$ is between that on Pt/Al_2O_3 and on Pt/CeO_2, and has a strong temperature and CO partial pressure dependence. Thus, it seems as if ceria in the $Pt/CeO_2/Al_2O_3$ catalyst is more difficult to reduce than ceria in the Pt/CeO_2 catalyst.

Modeling the Reduction of Pt/Ceria

The oxidation was too fast to be modeled from the experiments made in this study. However, the reduction was slower, which allowed modeling of the reduction step changes over Pt/ceria at two CO molar fractions (0.38 and 4.37%) and at two temperatures (300 and 400°C). Some features of the experiment helped us develop a model. On both ceria and Pt/ceria there was an immediate and nearly complete CO consumption; see Fig. 4. With Pt/ceria, about 2/3 of this CO consumption immediately appeared as CO_2 in the gas phase. On ceria, there was a slower CO_2 production, and a smaller part of the CO was converted to CO_2. Thus, there seemed to be two types of ceria reduction mechanisms, one faster which involves Pt and one slower without Pt. Moreover, since the CO_2 formation was always smaller than the CO consumption, there was some kind of accumulation of CO on ceria. We found that this CO accumulation was well described by a CO disproportionation reaction on ceria, which has been found to occur at room temperature over partially reduced CeO_2 (20). Daniel (21) observed CO dissociation also on Pt/CeO_2, but it was not seen by Jin *et al.* (22). Finally, since FT-IR data have shown the presence of carbonates on ceria under experimental conditions similar to ours (17), we also included carbonate formation in the model. After testing a number of models with the general features given above, we found that the CO step changes (i.e., the CO consumption and the CO_2 production) could be relatively well represented by the following model:

(1) At the beginning of the step (after the oxidation), there are a number of available oxygen atoms (independent of the temperature) at the ceria surface. This oxygen may be surface oxygen in the ceria lattice as well as adsorbed oxygen species.

(2) CO from the gas phase reacts with these oxygen sites to form adsorbed CO_2, with the rate

$$r_{CO_2,\text{ceria}} = k_{CO_2,\text{ceria}} \cdot c_{CO,g} \cdot \theta_O,$$

where $c_{CO,g}$ is the concentration of CO in the gas phase in mol/m^3 and θ_O is the fractional coverage of oxygen on the available oxygen sites.

(3) The formed CO_2 in reaction 2 above desorbs with the rate

$$r_{CO_2\,\text{des,ceria}} = k_{CO_2\,\text{des,ceria}} \cdot \theta_{CO_2}.$$

(4) CO adsorbs on the created oxygen vacancies at the surface:

$$r_{CO\,\text{ads,ceria}} = k_{CO\,\text{ads,ceria}} \cdot c_{CO,g} \cdot (1 - \theta_O - \theta_{CO_2} - \theta_{CO} - \theta_C).$$

(5) CO desorbs with the rate

$$r_{CO\,\text{des,ceria}} = k_{CO\,\text{des,ceria}} \cdot \theta_{CO}.$$

(6) CO disproportionation ($2\,CO \rightarrow C + CO_2$) takes place irreversibly between two adsorbed CO molecules:

$$r_{CO\,\text{dispr.}} = k_{\text{dispr.}} \cdot \theta_{CO}^2.$$

The reaction leaves carbon on one of the sites, which poisons this site, and CO_2 on the other site.

(7) The adsorbed CO_2 on ceria reacts irreversibly with an oxygen atom on ceria to produce cerium carbonate, which blocks two sites:

$$r_{\text{carbonate}} = k_{\text{carbonate}} \cdot \theta_{CO_2} \cdot \theta_O.$$

(8) CO adsorbs on Pt with the rate

$$r_{\mathrm{CO\,ads,Pt}} = k_{\mathrm{CO\,ads,Pt}} \cdot c_{\mathrm{CO,g}} \cdot (1 - \theta_{\mathrm{CO,Pt}}),$$

where $\theta_{\mathrm{CO,Pt}}$ is the coverage of CO on Pt.

(9) CO desorbs from Pt with the rate

$$r_{\mathrm{CO\,des,Pt}} = k_{\mathrm{CO\,des,Pt}} \cdot \theta_{\mathrm{CO,Pt}}.$$

(10) CO adsorbed on the metal reacts with O on ceria. The rate of this spillover reaction is

$$r_{\mathrm{CO_2,Pt-ceria}} = k_{\mathrm{CO_2,Pt-ceria}} \cdot \theta_{\mathrm{CO,Pt}} \cdot \theta_{\mathrm{O}}.$$

The produced CO_2 is assumed to immediately desorb from the Pt site, leaving a free Pt site and an oxygen vacancy.

(11) All rate coefficients k_i above can be described by Arrhenius expressions of the form

$$k_i = A_i \cdot \exp\left(-\frac{E_i}{R} \cdot \left(\frac{1}{T} - \frac{1}{T_m}\right)\right),$$

where T is the catalyst temperature and T_m is a reference temperature, both in K. The reference temperature was chosen to be 623 K.

Mass balances for all reacting species, with the assumptions above, resulted in a set of partial differential equations in the length coordinate and in time. These equations were discretisized by modeling the catalyst bed as a tank-series reactor, consisting of 10 ideal tank reactors. The resulting ordinary differential equations were solved in the commercial computer software MATLAB. A Levenberg–Marquardt routine was used to determine the optimal kinetic parameter values. The rate constants are based on the BET ceria surface area, the Pt surface area, and the Pt perimeter. The surface area of Pt was determined from the known metal loading, an approximate concentration of 1.25×10^{19} surface Pt atoms per metal area (23) and the measured Pt dispersion (value taken from second CO chemisorption after intermediate desorption at 300°C; see below). The Pt perimeter was estimated from the Pt loading, the Pt dispersion, and the BET ceria surface area, according to the formula (24)

$$I_0 = \frac{5.4 \times 10^{14} \cdot x_{\mathrm{Pt}} \cdot D^2}{\mathrm{BET}},$$

where I_0 is the Pt perimeter in m/m^2 support, x_{Pt} is the metal loading, D is the Pt dispersion, and BET is given in m^2/kg.

The measured and simulated step changes for 2.9% Pt/ceria with (a) 4.37% CO, 400°C; (b) 4.37% CO, 300°C; (c) 0.38% CO, 400°C; and (d) 0.38% CO, 300°C are shown in Fig. 5. The experiments and the model simulations show quite good correspondence. The model slightly underestimates the CO_2 formation, especially at the highest CO partial pressure. Moreover, there is a continuous CO

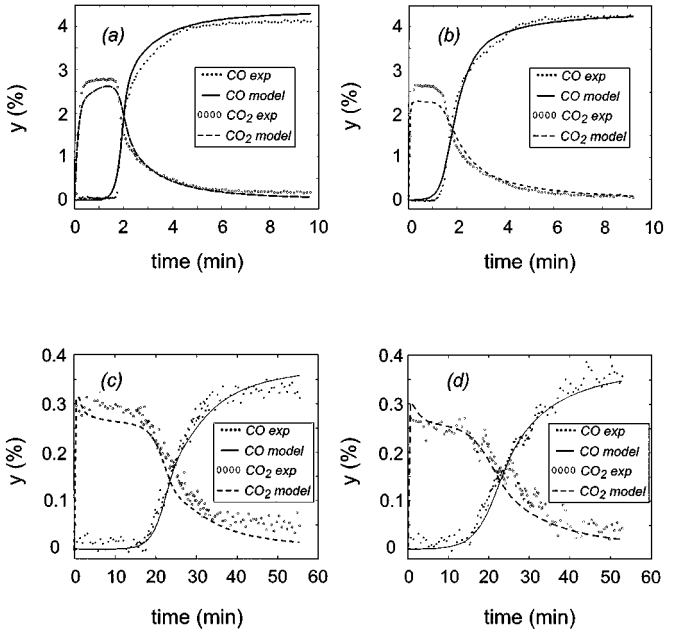

FIG. 5. Simulated and measured CO and CO_2 responses to a step change of CO on 2.9% Pt/ceria at (a) 400°C, 4.37% CO; (b) 300°C, 4.37% CO; (c) 400°C, 0.38% CO; and (d) 300°C, 0.38% CO.

consumption and CO_2 production, in particular in the experiment with 4.37% CO at 400°C, that the model does not take care of. The parameters and their individual 95% confidence intervals are shown in Table 3. The confidence intervals are generally quite large. Only for the parameters $A_{\mathrm{CO_2\,des,ceria}}$, $A_{\mathrm{CO_2,ceria}}$, $E_{\mathrm{CO_2,ceria}}$, $A_{\mathrm{CO\,dispr.,ceria}}$,

TABLE 3

The Parameters and Their 95% Confidence Intervals in the Model of the CO Step Changes on Pt/Ceria

Parameter	Value	95% confidence interval	Unit
$A_{\mathrm{CO\,ads,ceria}}$	7.6×10^{-6}	$\pm 6.7 \times 10^{-6}$	m^3/(s, m^2 ceria)
$E_{\mathrm{CO\,ads,ceria}}$	1.5	±2.5	kJ/mol
$A_{\mathrm{CO\,des,ceria}}$	7.0×10^{-7}	$\pm 6.1 \times 10^{-7}$	mol/(s, m^2 ceria)
$E_{\mathrm{CO\,des,ceria}}$	5.1	±5.7	kJ/mol
$A_{\mathrm{CO_2\,des,ceria}}$	1.7×10^{-7}	$\pm 0.44 \times 10^{-7}$	mol/(s, m^2 ceria)
$E_{\mathrm{CO_2\,des,ceria}}$	0.087	±18	kJ/mol
$A_{\mathrm{CO_2,ceria}}$	3.5×10^{-7}	$\pm 1.0 \times 10^{-7}$	m^3/(s, m^2 ceria)
$E_{\mathrm{CO_2,ceria}}$	110	±19	kJ/mol
$A_{\mathrm{CO\,dispr.,ceria}}$	3.2×10^{-8}	$\pm 0.65 \times 10^{-8}$	mol/(s, m^2 ceria)
$E_{\mathrm{CO\,dispr.,ceria}}$	24	±8	kJ/mol
$A_{\mathrm{carbonate,ceria}}$	4.9×10^{-10}	$\pm 20 \times 10^{-10}$	mol/(s, m^2 ceria)
$E_{\mathrm{carbonate,ceria}}$	0.044	±40	kJ/mol
$N_{\mathrm{O\,sites,ceria}}$	2.6×10^{-6}	$\pm 0.05 \times 10^{-6}$	mol/m^2 ceria
$A_{\mathrm{CO\,ads,Pt}}$	2.3×10^{-4}	$\pm 2.6 \times 10^{-4}$	m^3/(s, m^{2}Pt)
$E_{\mathrm{CO\,ads,Pt}}$	0.18	±0.3	kJ/mol
$A_{\mathrm{CO\,des,Pt}}$	2.2×10^{-4}	$\pm 2.6 \times 10^{-4}$	mol/(s, m^2 Pt)
$E_{\mathrm{CO\,des,Pt}}$	130	±92	kJ/mol
$A_{\mathrm{CO_2,Pt-ceria}}$	1.2×10^{-14}	$\pm 0.36 \times 10^{-14}$	mol/(s, m Pt perimeter)
$E_{\mathrm{CO_2,Pt-ceria}}$	1.0	±3.9	kJ/mol

$E_{CO\ dispr.,ceria}$, $N_{O\ sites,ceria}$, and $A_{CO_2,Pt-ceria}$ are the confidence intervals smaller than 35% of the parameter value. These parameters are thus the most important, since they have the largest impact on the solution. A second group is $A_{CO\ ads,ceria}$, $E_{CO\ ads,ceria}$, $A_{CO\ des,ceria}$, $E_{CO\ des,ceria}$, $A_{CO\ ads,Pt}$, $E_{CO\ ads,Pt}$, $A_{CO\ des,Pt}$, and $E_{CO\ des,Pt}$, for which the confidence intervals are of about the same magnitude as the parameters. For the parameters, $E_{CO_2\ des,ceria}$, $A_{carbonate,ceria}$, $E_{carbonate,ceria}$, and $E_{CO_2,Pt-ceria}$, the confidence interval is 4–1000 times larger than the parameter values. This means that the solution is not very sensitive to the value of these parameters. For some of the parameters, there are logical explanations for the large confidence intervals. An analysis of the coverages shows that the carbonate formation is small and that it could have been excluded from the model. This means that the two parameters describing the carbonate formation are not significant, which results in large confidence intervals. Moreover, the parameters $A_{CO\ ads,ceria}$ and $A_{CO\ des,ceria}$ are highly correlated (0.994), which means that they may be significant even though their confidence intervals are large. For all other parameters, the correlations are below 0.8.

Oxygen Exchange

After the initial oxidation, the exchange between oxygen isotopes starts, as can be seen in Fig. 2. ^{18}O from the gas phase replaces some of the ^{16}O in the catalyst. This exchange continues until all mobile oxygen has the same isotope ratio as oxygen in the gas phase, assuming that isotope effects can be neglected. During the oxygen exchange, there is no additional oxygen uptake on the catalyst, as can be seen from the constant level of the total oxygen concentration in Fig. 2. As a measure of the exchange rate, we will use the amount of oxygen exchanged during the first 10 min, $A_{10\,min}$, calculated as

$$A_{10\,min} = \frac{F_{tot}}{W}\int_0^{10}(2(y^{in\ 18}O_2 - y^{out\ 18}O_2) + y^{in\ 16}O^{18}O - y^{out\ 16}O^{18}O)dt,$$

where F_{tot} is the total molar flow rate, W is the catalyst mass, and y_i^{in} and y_i^{out} are the molar fractions of species i at the reactor inlet and outlet. $A_{10\,min}$ as a function of temperature for 2.5% Pt/Al_2O_3, 2.9% Pt/CeO_2 and CeO_2 (HS) is plotted in Fig. 6.

Exchange rate on Pt/Al_2O_3. The exchange rate was found to be highest on the Pt/alumina catalysts. On these samples, the exchange rate was a strong function of the number of Pt surface sites, the latter measured by CO chemisorption. This correlation is shown in Fig. 7, in which the oxygen exchange rate, $A_{10\,min}$ at 400°C is plotted against the number of Pt surface sites. The exchange rate was highest on 2.5% Pt/Al_2O_3. On pure alumina, there was no exchange, which shows that the exchange occurs through

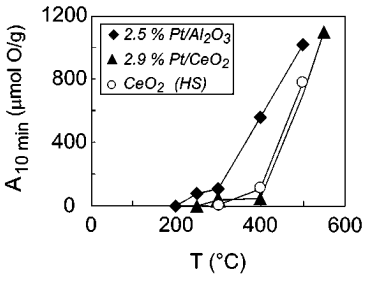

FIG. 6. Oxygen exchange during the first 10 min ($A_{10\,min}$) as a function of temperature.

Pt. The total amount exchanged was 3.1 atoms/nm^2 alumina at 400°C and 5.5 atoms/nm^2 alumina at 500°C. These figures correspond to the expected amount of oxygen in OH groups on alumina at these temperatures. The OH coverage should be between 6.2 OH groups/nm^2 (which is the saturation amount (9)) and 1.0 OH groups/nm^2 (which is the amount after dehydration at 800–1000°C (25)). Moreover, Duprez *et al.* (25) found that the oxygen exchange rate on Pt/alumina was proportional to the OH group coverage, which also supports the idea that the exchange proceeds via the OH groups.

Exchange rate on Pt/CeO_2. On oxidized ceria, the oxygen exchange was very slow at moderate temperatures (see Fig. 6) and independent of the Pt loading. However, very large amounts of oxygen were exchanged. At 300–400°C, the exchange was too slow to be completed within the experimental time. But when the temperature was increased to 600°C, the exchange was faster, and we were able to observe that about 50% of the oxygen in the ceria lattice had been exchanged. Since the gas phase contained 50% ^{18}O and 50% ^{16}O, this means that the exchange was complete, and that practically all oxygen atoms in the ceria are exchangeable at 600°C.

In the experiments in which the samples had been oxidized by $^{16}O_2$ instead of by the isotopic mixture, the oxygen exchange rate, $A_{10\,min}$, was approximately the same. This may seem surprising, since the amount of surface $^{16}O_2$

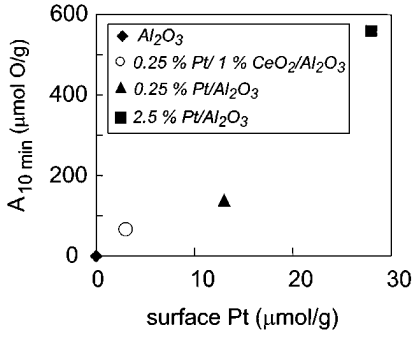

FIG. 7. Oxygen exchange during the first 10 min ($A_{10\,min}$) at 400°C as a function of surface Pt sites for the alumina-supported catalysts.

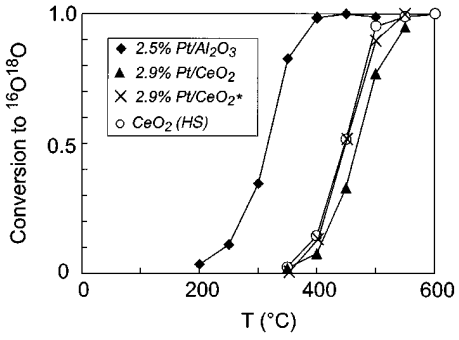

FIG. 8. Conversion to $^{16}O^{18}O$, expressed as the molar fraction of $^{16}O^{18}O$ relative to the equilibrium molar fraction of $^{16}O^{18}O$, as a function of temperature on 2.9% Pt/CeO_2, 2.9% Pt/CeO_2* (chlorine-free), 2.5% Pt/Al_2O_3, and CeO_2 (HS).

(which is most available to oxygen exchange) was in this case higher. The fact that an enrichment in $^{16}O_2$ at the surface does not increase the rate of exchange suggests that the mixing of oxygen isotopes in the ceria lattice is fast relative to the adsorption/desorption of oxygen. The surface would then, in the beginning of the exchange, be dominantly covered by ^{16}O for both cases, which explains the similar exchange rates.

Oxygen Equilibration

The rates of oxygen equilibration as a function of temperature on Pt/CeO_2, Pt/Al_2O_3, and CeO_2 are shown in Fig. 8. The rates are given as conversion to $^{16}O^{18}O$, which is here defined as the outlet concentration of $^{16}O^{18}O$ divided by the equilibrium concentration. The equilibrium concentration was calculated using the assumption that the equilibrium constant is four, i.e., that a mixture of equal amounts of ^{16}O and ^{18}O atoms should contain 25% $^{16}O_2$, 25% $^{18}O_2$, and 50% $^{16}O^{18}O$ (26). This assumption will lead, if the oxygen equilibration occurs through Langmuir–Hinshelwood type kinetics, to the following rate for the formation of $^{16}O^{18}O$ (in analogy with the analysis for the HD-formation according to Niklasson and Andersson (27)),

$$r_{1618} = -k_v\left(c_{^{16}O^{18}O} - c^{eq}_{^{16}O^{18}O}\right),$$

where k_v is the rate constant for the oxygen equilibration in m^3/(s, kg catalyst), $c_{^{16}O^{18}O}$ is the concentration of $^{16}O^{18}O$, and eq means at equilibrium. By modeling the catalyst bed as an ideal tubular reactor, k_V can be calculated as

$$k_v = -\frac{q}{W}\ln\left(\frac{c^{out}_{^{16}O^{18}O} - c^{eq}_{^{16}O^{18}O}}{c^{in}_{^{16}O^{18}O} - c^{eq}_{^{16}O^{18}O}}\right),$$

where q is the gas flow rate in m^3/s and W is the catalyst mass in kg. The index eq means at equilibrium, out at the reactor outlet, and in at the reactor inlet.

Figure 8 shows that the $^{16}O_2$, $^{18}O_2$ equilibration is fast on Pt/Al_2O_3 above 250°C. On Pt/CeO_2 and CeO_2, a temperature increase of 120–150°C is necessary to obtain the same conversion as on Pt/Al_2O_3. The Pt/CeO_2 samples, prepared from the chlorine-containing and from the chlorine-free (marked $*$) precursor, show similar behavior. This shows that chlorine residuals, which are expected to remain after calcination at 500°C, are not inhibiting the oxygen exchange. Such an inhibition was observed for Pt and Rh on alumina (28).

The apparent activation energy for the rate constant k_v was higher for Pt/CeO_2 and CeO_2, which both had 124 kJ/mol (the chlorine-free Pt/CeO_2 sample had an activation energy of 122 kJ/mol), compared to 71 kJ/mol for Pt/Al_2O_3. The pre-exponential factor in the Arrhenius expression is 3.6×10^{11} Å^3/(s, Pt sites) for Pt/Al_2O_3. For Pt/CeO_2 and CeO_2, it is more difficult to determine the number of "sites," since oxygen adsorption occurs both on Pt and on ceria. If we assume that each surface oxygen atom represents one site, the pre-exponential becomes 5.9×10^{11} Å^3/(s, Pt and ceria sites) for Pt/CeO_2 and 10×10^{11} Å^3/(s, ceria sites) for CeO_2. The frequency of site collisions is thus approximately the same on all materials, but there is a larger barrier toward the equilibration reaction on ceria and Pt on ceria. Surprisingly, Pt on ceria seems inactive for oxygen equilibration. This is in contrast to Pt on alumina, for which Pt is responsible for all oxygen equilibration at 400°C and below (we did not observe any oxygen equilibration on the bare alumina support at these temperatures). The equilibration rate is even somewhat higher on CeO_2 than on Pt/CeO_2. By neglecting the Pt contribution, and assuming that all oxygen adsorption occurs on ceria, this difference could be attributed to the 20% lower BET surface area of Pt/CeO_2 compared to CeO_2; see Table 1.

CO/H_2 Chemisorption and CO-TPD

On Pt/Al_2O_3, the CO and H_2 chemisorption measurements gave similar results; see Table 1. However, on Pt/CeO_2, the CO uptake was considerably higher than the H uptake. The CO uptake was even above 1 CO molecule per Pt atom on 0.3% Pt/CeO_2 (the stoichiometry is generally assumed to be about 0.7 adsorbed CO molecules per Pt surface atom (29)). Due to these high CO uptakes, the Pt/CeO_2 samples were investigated further. One might suspect that ceria also adsorbs CO. Yet there was no CO uptake on CeO_2 (LS) and very little on CeO_2 (HS), so the high CO uptake seemed to be due to Pt and ceria interacting in some spillover process. Our TPD measurements after CO adsorption at 25°C on Pt/CeO_2 showed two CO desorption peaks below 300°C, and one CO desorption peak above 300°C; see Fig. 9a. There was also some CO_2 desorption at about 500°C. The CO_2 peak could have originated from adsorbed CO, which removes oxygen from ceria at elevated temperatures. Another explanation is that the desorbed CO_2 originated from carbonate and carboxylate species, which have been observed during CO adsorption on ceria (15).

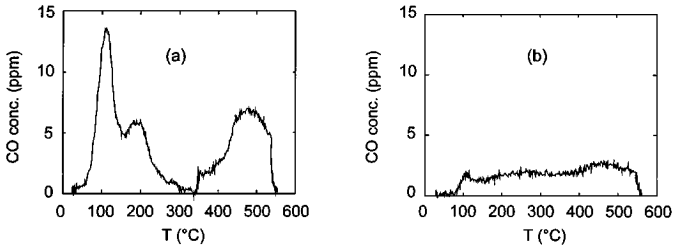

FIG. 9. TPD of CO adsorbed at 25°C on 2.9% Pt/CeO_2, (a) reduced in H_2 at 300°C and (b) reduced in H_2 at 650°C.

The CO_2 desorption peak temperature of 500°C corresponds to the decomposition temperature of cerium carbonate (30) and also to the desorption temperature of unidentate CO_2 on ceria (15).

The CO desorption peaks at 100–200°C are usually attributed to CO adsorbed on Pt (29), whereas the high-temperature CO peak has been attributed to CO adsorbed in the Pt/ceria interface (31). However, this does not explain a stoichiometry above one CO molecule per Pt atom, and, therefore, our hypothesis was to consider all CO and CO_2 desorption above 300°C to be of spillover type, associated with ceria. To subtract the spillover contribution, the CO chemisorption measurements were repeated, with a reduction at 300°C between the measurements. The reduction at 300°C was carried out so that CO on Pt would desorb, whereas CO and CO_2 on ceria would still be adsorbed. In this repeated measurement, the amount of CO chemisorption decreased by about 50%; see Table 4. We also measured the CO uptake at −78°C, a temperature which is expected to hinder a spillover process. The CO uptake at −78°C was also about 50% lower than at 25°C; see Table 4.

Finally, measurements were carried out after a high-temperature reduction at 650°C, which has been shown to result in a strong metal–support interaction (SMSI) (3, 6, 21). In these investigations, the SMSI took the form of a reversible (upon mild oxidation) decrease of the CO uptake after a high-temperature reduction. This behavior was also observed in our measurements; see Table 4. TPD after CO chemisorption at 25°C, after reduction in H_2 at 650°C, showed one broad CO desorption peak; see Fig. 9b. During this TPD, there was no CO_2 formation. The lack of CO_2 in this case was due to the fact that further reduction of ceria during the TPD was not possible, since the sample had already been reduced at a high temperature (650°C). Furthermore, it seems likely that carbonate formation is hindered on strongly reduced ceria. Golunski *et al.* (6) proposed that the diminished CO uptake after a high-temperature reduction was due to ceria migration to cover the Pt. However, such a covering has not been observed in TEM images of Pt/CeO_2 reduced at 500°C (32). Moreover, IR measurements on Pt/CeO_2, reduced at 700°C, have detected the presence of CO−Pt bonds, which shows that Pt is not covered with ceria (21). Instead an electronic SMSI has been suggested, partly supported by a small shift toward a lower binding energy of the CO−Pt bond (21).

One final comment should be made about the uncertainties in the hydrogen chemisorption measurements. One cannot exclude the possibility of hydrogen spillover from Pt to ceria, as has been reported for chlorine-free Rh/ceria at room temperature (33, 34). This means that hydrogen chemisorption may overestimate the metal dispersion. However, our data indicate that the overestimation is at least smaller than when CO chemisorption is used.

TABLE 4

CO Chemisorption at 25 or −78°C on 0.3% Pt/CeO_2

Pretreatment	CO/Pt at 25°C	CO/Pt at −78°C
H_2 300°C	1.4	0.7
H_2 300°C–CO 25°C–H_2 300°C	0.7	—
H_2 300°C–CO 25°C–H_2 300°C–CO 25°C–H_2 300°C	0.9	—
H_2 650°C	0.3	0.3
H_2 650°C–CO 25°C–H_2 300°C	0.2	—
H_2 650°C–O_2 300°C–H_2 300°C	1.2	—

DISCUSSION

Ceria is capable of storing large amounts of oxygen. For the high Pt-loading Pt/CeO_2 catalyst, the stored amount at 300–400°C roughly corresponds to 0.5 O atoms per surface Ce atom. This amount corresponds to surface ceria switching between the compositions CeO_2 and Ce_2O_3. If, on the other hand, the reduction is uniform in the entire ceria sample, the observed oxygen storage would correspond to a ceria composition of $CeO_{1.85}$ in the reduced form. However, this seems unlikely since the hydrogen uptake during TPR has been found to increase with increasing surface area of ceria (1, 35). Laachir *et al.* (19) also found that the hydrogen uptake during 2 h at 400°C increased with a larger surface area of the ceria sample. Only for very long reduction times (20 h at 400°C) was there such a high degree of reduction that it seemed to involve also bulk reduction. In contrast, Holgado and Munuera (36) found that the oxidation state of the ceria at the surface, measured by XPS, when compared with the hydrogen uptake during TPR, pointed to a uniform reduction of ceria. These authors suggested that the oxygen vacancies, although being created at the surface of the ceria, readily diffuse into the material, creating a homogenous distribution of vacancies.

From the reduction experiments with CO, it was seen that Pt facilitates the release of the stored oxygen at 300–400°C. Oxidation was found to occur very fast both on Pt-catalyzed ceria and on pure ceria, whereas the reduction was slower, and more dependent on the Pt to occur below 400°C. Both the amount and the rate of reduction were

higher in the presence of Pt. Our interpretation of these results is that reduction of ceria is the limiting factor for oxygen storage. This is consistent with measurements of noble-metal-promoted ceria/alumina catalysts in real exhaust conditions (13, 37), and also with measurements on pure ceria (12). A model of the reduction step changes on Pt/ceria was developed. The model is based on the observations of the dynamics of the CO consumption and the CO_2 production of ceria and Pt/ceria at two temperatures and two CO partial pressures. These observations indicate that there are three mechanisms for CO_2 formation, two involving removal of oxygen from ceria and the third involving CO disproportionation. Carbonate formation is also included in the model. Both CO disproportionation (20) and carbonate formation (15–17) have been observed on ceria. However, we have not shown by independent measurement that these reactions are important in our experiments. Therefore, we do not claim that the model is physically correct, only that it fits our data reasonably well, and that it can be used as a starting point for further studies. The confidence intervals of the parameters were also high, which demonstrates the uncertainties of the model.

We observed large amounts of exchange between ^{18}O in gas phase and ^{16}O in the catalyst on the oxidized Pt/CeO_2 and CeO_2 catalysts, but the exchange was slow. On alumina-supported catalysts, the exchange, which probably occurs with the OH groups on the alumina, was faster. The exchange and equilibration rates were closely related on all samples and the exchange rate was not increased by a surface enrichment of exchangeable ^{16}O. These observations show that oxygen adsorption and desorption are the rate-determining steps in the exchange, and not the oxygen diffusion. This agrees with results from Abderrahim and Duprez (9), and also means that Pt on alumina is more efficient than Pt on ceria in dissociating oxygen in oxidizing atmosphere.

The high oxygen-storage capacity of ceria was seen both on Pt/CeO_2 and on $Pt/CeO_2/Al_2O_3$. However, the efficiency (expressed as oxygen atoms that could be inserted and released per cerium oxide molecule) was lower in $Pt/CeO_2/Al_2O_3$. This lower efficiency of ceria together with alumina could be due to the lower surface area of the ceria in the $Pt/CeO_2/Al_2O_3$ sample; see Table 1. Another possible explanation is that in the mixed support sample, an intimate Pt/ceria contact is partially hindered by the presence of alumina. The high rate of oxygen exchange on $Pt/CeO_2/Al_2O_3$ is also an indication that most of the Pt is deposited on alumina.

The oxygen equilibration reaction was found to be fast on Pt/Al_2O_3 at 300°C, but very slow at 200°C and below. On Pt/CeO_2 and CeO_2, 420–450°C is needed to obtain the same conversion as on Pt/Al_2O_3 at 300°C. The slow reaction rate on Pt/CeO_2 and CeO_2 indicates that Pt on ceria, at least when oxidized, is practically inactive for oxygen dissociation, or at least not more active than ceria itself. Thus, the exchange seems to occur directly on ceria. These results indicate a strong electronic effect between Pt and ceria, i.e., that the oxygen–Pt bond strength is increased due to Pt–ceria interaction. The Pt dispersion is also very high, see Table 1, which means that the Pt particles are small and such a strong interaction is possible.

Pt/ceria has a low activity for oxygen dissociation compared to Pt/alumina. This may seem surprising, since the light-off temperatures for preoxidized Pt/ceria/alumina and Pt/alumina have been found to be about the same (5), whereas prereduced Pt/ceria and Pt/ceria/alumina has a higher activity compared to Pt/alumina (3, 5, 6). However, in the case of ceria, oxygen does not have to be supplied by the gas phase, but can come from ceria as well. Moreover, during the oxidation, CO reacting with oxygen desorbs as CO_2, leaving a new site for oxygen dissociation. One should also note that the low activity for oxygen dissociation was obtained for *oxidized* Pt dispersed on ceria. There may be a large difference between the activity between oxidized and reduced noble metal, as shown in studies of oscillations during oxidation of CO, reviewed by van Santen and Niemantsverdriet (38). Pt(110) is able to switch between two structures of different activity for O_2 adsorption. It has been shown that, at low CO coverage, the surface reconstructs to a form on which O_2 can hardly adsorb. At higher CO coverage, the surface reconstructs back to the more active form. These results, of course, cannot be extrapolated to our supported catalyst. They are mentioned only to indicate the possibility of surface reconstructions during oxidation/reduction, which may dramatically alter the catalytic properties.

The present study has also shown that CO chemisorption may be an inaccurate method to measure the Pt dispersion on CeO_2, due to some kind of CO spillover. Our measurements of H_2 chemisorption gave lower values of the Pt dispersion. We propose that, if CO is used for determining the Pt dispersion, the measurements should be repeated until CeO_2 is saturated with CO. By this procedure, the CO uptake decreases to about the same levels as the H uptake. However, further investigations of the possible use of this method are needed.

CONCLUSIONS

- The oxidation was fast (on a 0.1-s time scale) on all samples.
- Ceria has a high oxygen-storing capacity, but Pt is necessary to facilitate the removal of the stored oxygen at 300–400°C.
- A model of the reduction by CO of Pt/ceria is presented. The model contains 19 parameters and was shown to fit the data relatively well. The key features of the model are two types of reduction reactions (one involving CO from the gas phase and one with CO adsorbed on Pt), CO

disproportionation which poisons the ceria surface, and carbonate formation between CO_2 and oxygen.

- Adsorption/desorption of oxygen are the rate-determining steps in the oxygen exchange on oxidized Pt/CeO_2, $Pt/CeO_2/Al_2O_3$, Pt/Al_2O_3, and CeO_2 catalysts at 200–600°C.
- The oxygen exchange rate on oxidized Pt/CeO_2 is very low and independent of Pt content.
- The oxygen exchange rate on oxidized Pt/Al_2O_3 is high and strongly dependent on Pt content.
- Oxygen dissociation is fast on oxidized Pt/Al_2O_3. It is slower on Pt/CeO_2 and does not seem to occur on Pt.
- CO chemisorption to determine the Pt dispersion on ceria is an unreliable method due to CO uptake by ceria.

ACKNOWLEDGMENTS

Dr. Gudmund Smedler and Professor Bengt Kasemo at the Competence Center for Catalysis (KCK) are gratefully acknowledged for valuable comments on the manuscript. The authors also thank Leif Backman at the Helsinki University of Technology for performing the H_2 chemisorption measurements, and Dr. Magnus Skoglund and Peter Lööf for providing the catalyst samples. The Swedish National Board for Industrial and Technological Development is acknowledged for financial support.

REFERENCES

1. Yao, H. C., and Yu Yao, Y. F., *J. Catal.* **86**, 254 (1984).
2. Harrison, B., Diwell, A. F., and Hallett, C., *Platinum Met. Rev.* **32**(2), 73 (1988).
3. Diwell, A. F., Rajaram, R. R., Shaw, H. A., and Truex, T. J., *in* "Catalysis and Automotive Pollution Control II" (A. Crucq, Ed.), Studies in Surface Science and Catalysis, Vol. 71, p. 139. Elsevier, Amsterdam, 1991.
4. Yu Yao, Y. F., *J. Catal.* **87**, 152 (1984).
5. Serre, C., Garin, F., Belot, G., and Maire, G., *J. Catal.* **141**, 9 (1993).
6. Golunski, S. E., Hatcher, H. A., Rajaram, R. R., and Truex, T. J., *Appl. Catal. B* **5**, 367 (1995).
7. Nunan, J. G., Robota, H. J., Cohn, M. J., and Bradley, S. A., *J. Catal.* **133**, 309 (1992).
8. Boreskov, G. K., *in* "Catalysis—Science and Technology" (J. R. Anderson and M. Boudart, Eds.), Vol. 3, p. 56. Springer-Verlag, Berlin, 1982.
9. Abderrahim, H., and Duprez, D., *in* "Catalysis and Automotive Pollution Control" (A. Crucq and A. Frennet, Eds.), Studies in Surface Science and Catalysis, Vol. 30, p. 359. Elsevier, Amsterdam, 1987.
10. Rosynek, M. P., *Catal. Rev. Sci. Eng.* **16**(1), 111 (1977); and references therein.
11. Martin, D., Taha, R., and Duprez, D., *in* "Catalysis and Automotive Pollution Control III" (A. Frennet and J.-M. Bastin, Eds.), Studies in Surface Science and Catalysis, Vol. 96, p. 801. Elsevier, Amsterdam, 1995.
12. Padeste, C., Cant, N. W., and Trimm, D. L., *Catal. Lett.* **18**, 305 (1993).
13. Schlatter, J. C., and Mitchell, P. J., *Ind. Eng. Chem. Prod. Res. Dev.* **19**, 288 (1980).
14. Taha, R., Duprez, D., Mouaddib-Moral, N., and Gauthier, C., *in* "Fourth International Congress on Catalysis and Automotive Pollution Control" (N. Kruse, A. Frennet, and J.-M. Bastin, Eds.), Brussels, Belgium, April 9–11, 1997.
15. Li, C., Sakata, Y., Arai, T., Domen, K., Maruya, K., and Onishi, T., *J. Chem. Soc. Faraday Trans. 1* **85**(4), 929 (1989).
16. Artamonov, E. V., and Sazonov, L. A., *Kinet. Katal.* **12**(4), 961 (1971).
17. Breysse, M., Guenin, M., Claudel, B., and Veron, J., *J. Catal.* **28**, 54 (1973).
18. Bak, K., and Hilaire, L., *Appl. Surf. Sci.* **70/71**, 191 (1993).
19. Laachir, A., Perrichon, V., Badri, A., Lamotte, J., Catherine, E., Lavalley, J.-C., El Fallah, J., Hilaire, L., le Normand, F., Quéméré, E., Sauvion, G. N., and Touret, O., *J. Chem. Soc. Faraday Trans.* **87**(10), 1601 (1991).
20. Li, C., Sakata, Y., Arai, T., Domen, K., Maruya, K., and Onishi, T., *J. Chem. Soc. Chem. Commun.*, 410 (1991).
21. Daniel, D. W., *J. Phys. Chem.* **92**, 3891 (1988).
22. Jin, T., Okuhara, T., Mains, G. J., and White, J. M., *J. Phys. Chem.* **91**, 3310 (1987).
23. Anderson, J. R., "Structure of Metallic Catalysts," p. 296. Academic Press, London, 1975.
24. Duprez, D., *in* "Proc. 4th Int. Conf. Spillover" (Can Li and Qin Xin, Eds.), p. 13. Elsevier, Amsterdam, 1997.
25. Duprez, D., Abderrahim, S., Kacimi, S., and Rivière, J., *in* "Proc. 2nd Int. Conf. Spillover" (K. H. Steinberg, Ed.), p. 127. Karl Marx-Universität, Leipzig, 1989.
26. Klier, K., Nováková, J., and Jíru, P., *J. Catal.* **2**, 479 (1963).
27. Niklasson, C., and Andersson, B., *Ind. Eng. Chem. Res.* **27**, 1370 (1988).
28. Abderrahim, H., and Duprez, D., *in* "Proceedings, 9th International Congress on Catalysis, Calgary, 1988" (M. J. Phillips and M. Ternan, Eds.), Vol. 3, p. 1246. Chem. Institute Canada, Ottawa, 1988.
29. Kasemo, B., and Törnqvist, E., *Phys. Rev. Lett.* **44**(23), 1555 (1980).
30. Kirk-Othmer, "Encyclopedia of Chemical Technology," 3rd ed., Vol. 5, p. 322. Wiley, New York, 1979.
31. Lööf, P., Kasemo, B., Andersson, S., and Frestad, A., *J. Catal.* **130**, 181 (1991).
32. Datye, A. K., Kalakkad, D. S., Yao, M. H., and Smith, D. J., *J. Catal.* **155**, 148 (1995).
33. Bernal, S., Calvino, J. J., Cifredo, G. A., Rodríguez-Izquierdo, J. M., Perrichon, V., and Laachir, A., *J. Catal.* **137**, 1 (1992).
34. Bernal, S., Calvino, J. J., Cifredo, G. A., Gatica, J. M., Pérez Omil, J. A., Laachir, A., and Perrichon, V., *in* "Catalysis and Automotive Pollution Control III" (A. Frennet and J.-M. Bastin, Eds.), Studies in Surface Science and Catalysis, Vol. 96, p. 419. Elsevier, Amsterdam, 1995.
35. Johnson, M. F. L., and Mooi, J., *J. Catal.* **103**, 502 (1987).
36. Holgado, J. P., and Munuera, G., *in* "Catalysis and Automotive Pollution Control III" (A. Frennet and J.-M. Bastin, Eds.), Studies in Surface Science and Catalysis, Vol. 96, p. 109. Elsevier, Amsterdam, 1995.
37. Herz, R. K., *Ind. Eng. Chem. Prod. Res. Dev.* **20**, 451 (1981).
38. van Santen, R. A., and Niemantsverdriet, J. W., "Chemical Kinetics and Catalysis" (M. W. Twigg and M. S. Spencer, Eds.), Fundamental and Applied Catalysis, p. 66. Plenum Press, New York, 1995.